ComEX

IEICE Communications Express, Vol.8, No.4, 122–128

Experimental study on polarimetric-HoloSAR

Hiroki Shimoda[a)], **Yoshio Yamaguchi, and Hiroyoshi Yamada**

Graduate School of Science & Technology, Niigata University,
Ikarashi 2–8050, Nishi-ku, Niigata 950–2181, Japan

a) *shimoda@wave.ie.niigata-u.ac.jp*

Abstract: This paper pursuits a possibility of fully polarimetric and three-dimensional (3-D) imaging by Holographic Synthetic Aperture Radar Tomography (HoloSAR). HoloSAR is 3-D extension of Circular Synthetic Aperture Radar (CSAR) along the vertical direction whose trajectory is a circle in a horizontal plane. By adding fully polarimetric capability to HoloSAR, it becomes a perfect 3-D imaging radar system which reveals scattering mechanisms from object through scattering power decomposition. This paper attempts to achieve such a prototype system in an anechoic chamber. The experimental result successfully yielded a 3-D image reconstruction of objects with exhibiting polarimetric scattering mechanism.

Keywords: Synthetic Aperture Radar (SAR), CSAR, HoloSAR, scattering mechanism

Classification: Sensing

References

[1] A. Moreira, P. Prats-Iraola, M. Younis, G. Krieger, I. Hajnsek, and K. P. Papathanassiou, "A tutorial on synthetic aperture radar," *IEEE Geosci. Remote Sens. Mag.*, vol. 1, no. 1, pp. 6–43, Mar. 2013. DOI:10.1109/MGRS.2013.2248301

[2] O. Ponce, P. Prats-Iraola, R. Scheiber, A. Reigber, and A. Moreira, "First airborne demonstration of Holographic SAR Tomography with fully polarimetric multicircular acquisitions at L-band," *IEEE Trans. Geosci. Remote Sens.*, vol. 54, no. 10, pp. 6170–6196, Oct. 2016. DOI:10.1109/TGRS.2016.2582959

[3] J.-S. Lee, E. Pottier, *Polarimetric Radar Imaging: From Basics to Applications*, CRC Press, Feb. 2009.

[4] A. Moriya, H. Yamada, Y. Yamaguchi, "Fundamental considerations on polarimetric step-frequency radar," Tech. Rep. of IEICE SANE95-77, Oct. 1995.

[5] Y. Yamaguchi, T. Moriyama, M. Ishido, and H. Yamada, "Four-component scattering model for polarimetric SAR image decomposition," *IEEE Trans. Geosci. Remote Sens.*, vol. 43, no. 8, pp. 1699–1706, Aug. 2005. DOI:10.1109/TGRS.2005.852084

[6] C. Ozdemir, *Inverse Synthetic Aperture Radar Imaging with MATLAB Algorithms*, John Wiley & Sons, 2012.

DOI: 10.1587/comex.2018XBL0153
Received December 11, 2018
Accepted January 25, 2019
Publicized February 8, 2019
Copyedited April 1, 2019

1 Introduction

With the advent of Synthetic Aperture Radar (SAR), various functions to SAR systems and data acquisition methods have been applied and added to improve the system performances. Recent SAR advances are well explained in [1], including polarimetry, interferometry, tomography, etc. One goal of SAR applications will be 3-D reconstruction of objects under imaging. Since precise 2-D imaging around 360° is available now by Circular SAR whose trajectory is circular in a horizontal plane, it will be possible to use multiple CSAR in the vertical direction for 3-D imaging.

The pioneering HoloSAR work [2] explains the principle and 3-D reconstruction method in detail together with related problems. This work intends the HoloSAR by adding polarimetric scattering power decomposition scheme [3] to achieve advanced 3-D image reconstruction system. If this kind of Polarimetric-HoloSAR system becomes available, precise 3-D image reconstruction with scattering mechanisms will be available for future applications.

In the following, a brief HoloSAR principle using backprojection method is described in Sect. 2, followed by polarimetric scattering power decomposition scheme in Sect. 3, and the experimental results in Sect. 4. Sect. 5 is the conclusion.

2 HoloSAR methodlogy

Among various CSAR schemes, we use Step Frequency Continuous Wave (SF-CW) radar system [4] for the measurement based on a vector network analyzer.

2.1 Formulation

Fig. 1 shows the HoloSAR measurement configuration. The aspect angle φ, and height Z_c are defined as

$$\varphi = k\Delta\varphi \quad (k = 0, 1, 2 \ldots, N_\varphi) \tag{1}$$

$$Z_c = Z_{min} + l\Delta Z_c \quad (l = 0, 1, 2 \ldots, N_{Z_c}) \tag{2}$$

where $\Delta\varphi$ and ΔZ_c are sampling intervals, N_φ, N_{Z_c} are number of sampling points, and Z_{min} is the minimum height. Step frequency f is defined by

$$f = f_0 - \frac{B}{2} + m\frac{B}{N_f} \quad (m = 0, 1, 2 \ldots, N_f) \tag{3}$$

where f_0 is the center frequency, B is bandwidth, and N_f is number of steps. Transmitted impulse signal s of SF-CW radar is written as

$$s(t, \omega) = \exp(j\omega t). \tag{4}$$

In the model shown in Fig. 1, the received signal p for the point target (x_n, y_n, z_n). p is represented by

$$p(t, \omega, \varphi, Z_c) = \sum_{n=1}^{N_{tgt}} g_n \exp\{j\omega[t - \tau_n(\varphi, Z_c)]\} \tag{5}$$

where N_{tgt} is number of point objects, g_n is reflection coefficient, τ_n is round trip time delay from antenna position to the position (x_n, y_n, z_n) of object n. The time delay τ_n is represented by

DOI: 10.1587/comex.2018XBL0153
Received December 11, 2018
Accepted January 25, 2019
Publicized February 8, 2019
Copyedited April 1, 2019

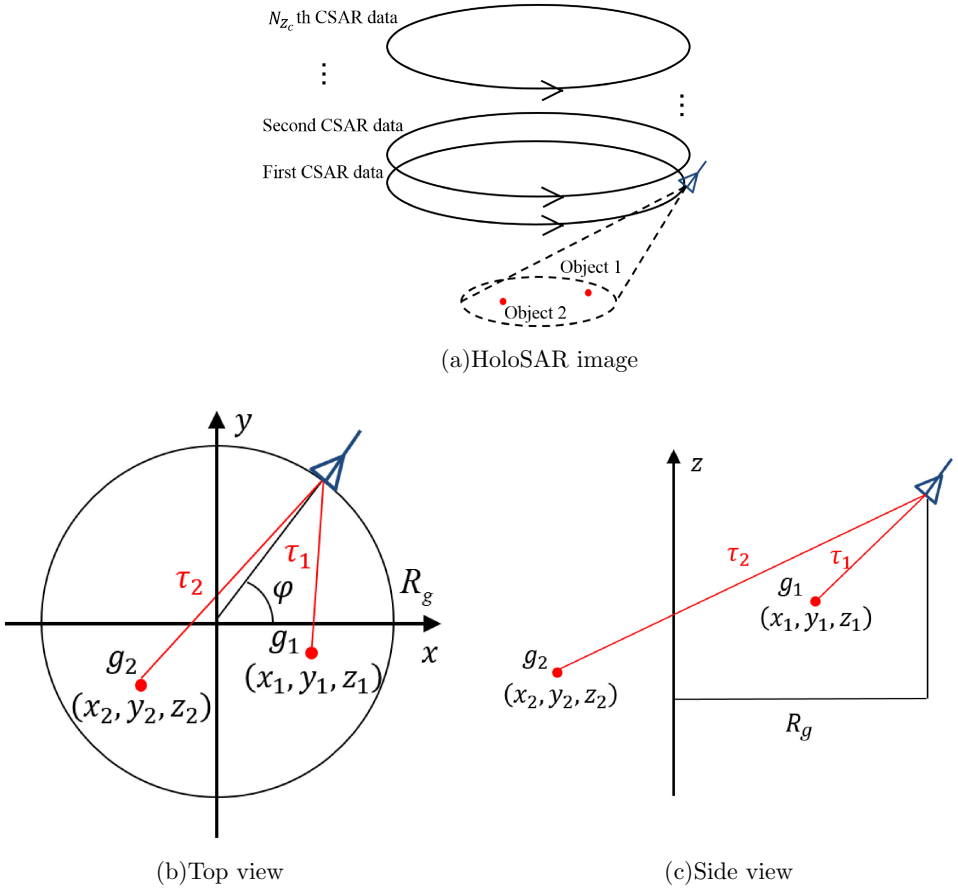

Fig. 1. System model

$$\tau_n(\varphi, Z_c) = \frac{2\sqrt{(x_n - R_g\cos\varphi)^2 + (y_n - R_g\sin\varphi)^2 + (z_n - Z_c)^2}}{c} \tag{6}$$

where R_g is trajectory radius. The transmission and reception ratio S becomes

$$S(\omega, \varphi, Z_c) = \frac{p(t, \omega, \varphi, Z_c)}{s(t, \omega, \theta, Z_c)} = \sum_{n=1}^{N_{tgt}} g_n \exp\{-j\omega\tau_n(\varphi, Z_c)\}. \tag{7}$$

The HoloSAR reconstruction is achieved by calculating g in (8) using the back-projection method. g is represented by

$$g(x, y, z) = \frac{\sum_{k=0}^{N_f}\sum_{l=0}^{N_\varphi}\sum_{m=0}^{N_{Z_c}} S(\omega, \varphi, Z_c)\exp\{j\omega t(x, y, z, \varphi, Z_c)\}}{N_f N_\varphi N_{Z_c}} \tag{8}$$

$$t(x, y, z, \varphi, Z_c) = \frac{2\sqrt{(x - R_g\cos\varphi)^2 + (y - R_g\sin\varphi)^2 + (z - Z_c)^2}}{c} \tag{9}$$

where t in exponential term is round trip time delay from antenna position to space (x, y, z).

2.2 Image reconstruction

HoloSAR reconstruction is implemented with the following steps using back-projection scheme.

DOI: 10.1587/comex.2018XBL0153
Received December 11, 2018
Accepted January 25, 2019
Publicized February 8, 2019
Copyedited April 1, 2019

1. Range compression of raw data

$$S_{(t)} = \mathcal{F}_{(\omega)}[S(\omega, \varphi, Z_c)]^{-1}$$

where, $\mathcal{F}_{(\omega)}[.]^{-1}$ is fast time inverse Fourier transform.

2. Approximation of round trip time delay from antenna position to space

$$t(x, y, z, \varphi, Z_c) \fallingdotseq t'(x_p, y_q, z_r, \varphi, Z_c) = \frac{2\sqrt{(x_p - R_g\cos\varphi)^2 + (y_q - R_g\sin\varphi)^2 + (z_r - Z_c)^2}}{c}$$

where, x_p, y_q, z_r are represented as followed using size of one boxel $\Delta x \times \Delta y \times \Delta z$.

$$x_p = x_{min} + p\Delta x \quad (p = 0, 1, 2 \ldots N_p)$$
$$y_q = y_{min} + q\Delta x \quad (q = 0, 1, 2 \ldots N_q)$$
$$z_r = z_{min} + r\Delta x \quad (r = 0, 1, 2 \ldots N_r)$$

where, $x_{min}, y_{min}, z_{min}$ are minimum analysis area, N_p, N_q, N_r are number of boxels in each direction.

3. Taking the sum

$$g(x_p, y_q, z_r) = \frac{\sum_{l=0}^{N_\varphi}\sum_{m=0}^{N_{Z_c}} S_{(t)}(\omega, \varphi, Z_c)\exp\{j\omega t'(x_p, y_q, z_r, \varphi, Z_c)\}}{N_\varphi N_{Z_c}}.$$

3 Polarimetric scattering power decomposition

By the polarimetric measurement using the combination of Tx and Rx with H-pol. and V-pol. basis, it is possible to obtain scattering matrix. This matrix can be transferred to Pauri vector,

$$\mathbf{k}_P = \frac{1}{\sqrt{2}}\begin{bmatrix} O_{HH} + O_{VV} \\ O_{HH} - O_{VV} \\ 2O_{HV} \end{bmatrix} \tag{10}$$

where O_{HH}, O_{HV}, O_{VH}, O_{VV} are observed scattering matrix elements after the reconstruction processing. The Pauli vector is used to create coherency matrix which retain the second order statistics of polarimetric information. The ensemble average of the coherency matrix, denoted as $\langle[T]\rangle$, is defined by,

$$\langle[T]\rangle = \frac{1}{N_{ave}}\sum^{N_{ave}}\mathbf{k}_P\mathbf{k}_P^\dagger = \begin{bmatrix} T_{11} & T_{12} & T_{13} \\ T_{21} & T_{22} & T_{23} \\ T_{31} & T_{32} & T_{33} \end{bmatrix} \tag{11}$$

where † is complex conjugate and transpose, and N_{ave} is the number of averaged boxels. The scattering power decomposition method expand the measured coherency matrix into sub-matrices representing scattering models [5], as follows:

$$\langle[T]\rangle = f_s[T]_{surface} + f_d[T]_{double} + f_v[T]_{volume} + f_c[T]_{helix}. \tag{12}$$

By comparing the quantity of the measured data and scattering model, we can retrieve the following 4-scattering powers to be used in the next section.

DOI: 10.1587/comex.2018XBL0153
Received December 11, 2018
Accepted January 25, 2019
Publicized February 8, 2019
Copyedited April 1, 2019

The surface scattering power P_s (Blue color assigned)
The double bounce power P_d (Red)
The volume scattering power P_v (Green)
The helix scattering power P_c (Yellow)

4 Experimental results

In this section, we pursuit a possibility of Polarimetric-HoloSAR to retrieve scattering mechanism from reconstructed images of concrete blocks in an echoic chamber measurement.

4.1 Measurement specification

Measurement specifications and object configuration are shown in Fig. 2. We used several concrete blocks with cube of 0.1 m, placed on an iron plate. The combination of these blocks were modeled as a building, collapsed building, and four isolated houses as shown in Fig. 2(b) for top view. Fig. 2(c) is a photo taken from $\varphi = 0°$, along the x axis of Fig. 2(b). Fig. 2(d) is a model of collapsed building whose maximum height is 0.3 m. Elevation angle of four isolated houses are 0°, 10°, 20°, 30° from the top of Fig. 2(b) with respect to x-axis. The origin of antenna height is set on the iron plate surface at $z = 0$. At each height, we used Inverse SAR (ISAR) scheme [6] to obtain fully polarimetric data set in a horizontal plane with circular trajectory.

Center frequency	15 GHz
Bandwidth	4 GHz
Number of steps	401 steps
Off-nadir angle	60°
Trajectory radius	2.25 m
Height interval	0.02 m
Antenna height	0.8∼1.8 m
Aspect angle interval	0.2°

(a)Radar parameters

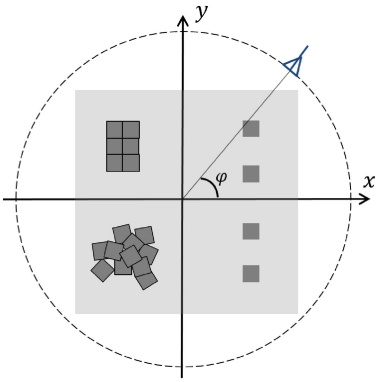

(b)Top view installation

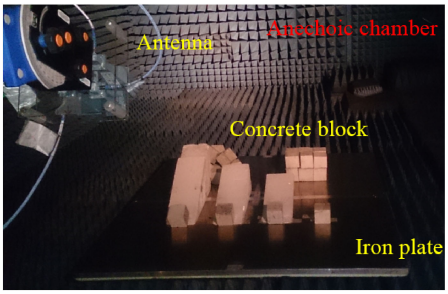

(c)Photo seen from the x-axis

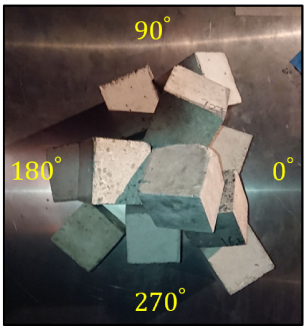

(d)collapsed building model

Fig. 2. Experimental situation

DOI: 10.1587/comex.2018XBL0153
Received December 11, 2018
Accepted January 25, 2019
Publicized February 8, 2019
Copyedited April 1, 2019

4.2 3-D image reconstruction

The data sets of fully polarimetric data by HoloSAR measurement were used to create 3-D image using the following parameters,

Size of one boxel: $\Delta x \times \Delta y \times \Delta z = 0.01 \times 0.01 \times 0.01$ [m]

Analysis area: $-1 \leq x \leq 1$, $-1 \leq y \leq 1$, $-0.5 \leq z \leq 0.5$ [m]

Averaging size: $x \times y \times z = 3 \times 3 \times 3$ [boxel]

Threshold: maximum power [dB] -20 [dB]

Fig. 3 shows a 3-D and fully polarimetric scattering power image of the scene under test (Fig. 2). The movie file Fig. 3(a) shows the reconstructed image viewed from 360° directions. Fig. 3(b) shows the image seen from top, while (c) is side view image (seen at $\varphi = 0°$).

As can be seen in Fig. 3, the image shows accurate mapping in the horizontal plane. The plotted box position is corresponding to the actual position in the measurement situation. The accurate 2-D positioning is the most advantageous of multi-lateral observations of HoloSAR.

The second advantage is an estimation of the maximum object height by vertical information of HoloSAR measurement. Also in the block with elevation

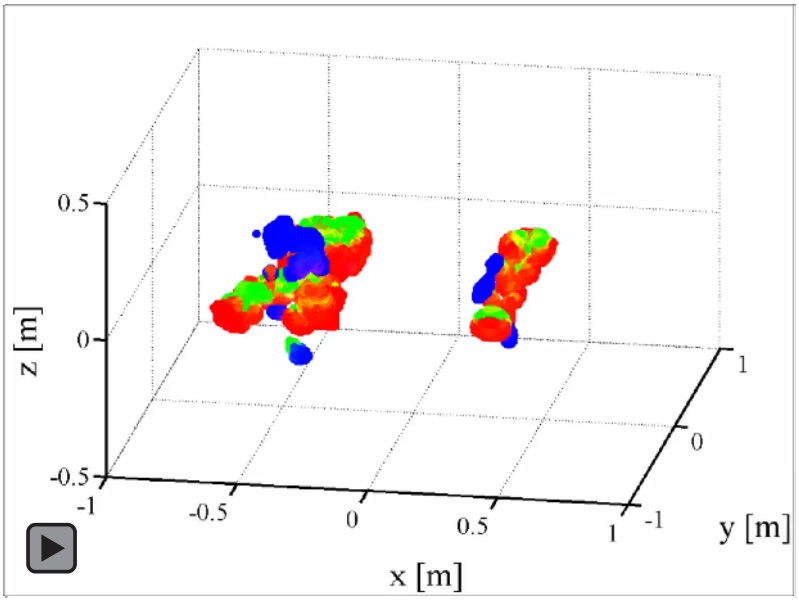

(a)Movie file seen from 360° directions

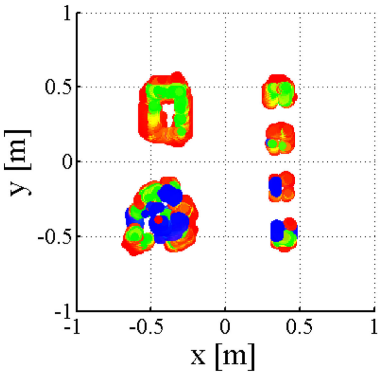

(b)Top view

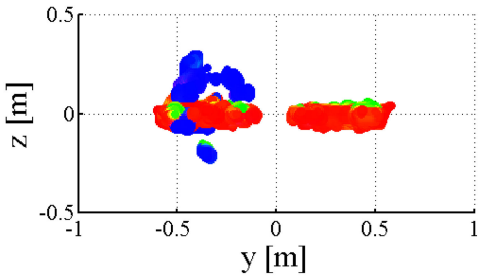

(c)Side view

Fig. 3. Polarimetric reconstruction image of Fig. 2.

DOI: 10.1587/comex.2018XBL0153
Received December 11, 2018
Accepted January 25, 2019
Publicized February 8, 2019
Copyedited April 1, 2019

angles of 20° and 30°, strong surface scattering P_s is seen. Since the elevation angle of a typical houses are 15° to 30°, the house height can be detected.

These above two advantages may be common to HoloSAR systems. The most important and third advantage of Polarimetric-HoloSAR is correct building detection capability by strong scattering power P_d caused by the double bounce scattering mechanism. By circular trajectory observation, it is possible to receive very strong double bounce scattering generated by the right angle structure of building walls and the ground. This happens four times if the building is rectangular. By adding the polarimetric capability, it becomes possible to classify or identify objects more accurately.

5 Conclusion

In this paper, we examined the possibility of fully polarimetric and HoloSAR to retrieve 3-D scattering information from objects under imaging scene. Basic experimental results showed advantages of HoloSAR for 1) accurate 2-D positioning in the horizontal plane, and 2) height information in the vertical direction. Furthermore, by polarimetric measurement, the capability of scattering mechanism information retrieval is added to the HoloSAR system, which leads to classify or identify objects accurately. If this kind of polarimetric HoloSAR systems becomes available, precise 3-D image reconstruction will be available for future applications.

DOI: 10.1587/comex.2018XBL0153
Received December 11, 2018
Accepted January 25, 2019
Publicized February 8, 2019
Copyedited April 1, 2019